Hindawi
International Journal of Photoenergy
Volume 2020, Article ID 6535372, 18 pages
https://doi.org/10.1155/2020/6535372

*Research Article*

# A New MPPT Technique for Fast and Efficient Tracking under Fast Varying Solar Irradiation and Load Resistance

**Libin Xu, Ruofa Cheng, and Jiajing Yang**

*School of Information Engineering, Nanchang Hangkong University, Nanchang, Jiangxi 330000, China*

Correspondence should be addressed to Ruofa Cheng; rfcheng36@126.com

Received 9 November 2019; Revised 25 December 2019; Accepted 17 January 2020; Published 4 February 2020

Academic Editor: Pierluigi Guerriero

Copyright © 2020 Libin Xu et al. This is an open access article distributed under the Creative Commons Attribution License, which permits unrestricted use, distribution, and reproduction in any medium, provided the original work is properly cited.

The maximum power point tracking (MPPT) is a strategy that allows imposing the PV array operation point on the maximum power point (MPP) or close to it under any environmental condition. The conventional incremental conductance (INC) algorithm is the most popular algorithm. But due to the fixed step size, its response speed is low under the rapid change of the solar irradiation level or load resistance. In this paper, a new MPPT technique is proposed to enhance the response speed. It consists of two stages: (1) the computing stage and (2) the regulating stage. The computing stage includes the coarse positioning operation and fine positioning operation. And an initial value of the duty cycle is generated in the computing stage, according to the characteristics of the DC-DC converter and the characteristics of the *I*-*V* curve. The regulating stage regulates the duty cycle of the DC-DC converter with a small step size, which can improve the tracking efficiency. And the computing stage can enhance the response speed. A simulation comparison of the proposed MPPT technique with other techniques is carried out in MATLAB/Simulink under different scenarios. The simulation results reveal that the response of the proposed algorithm is 4.6 times faster than that of the INC under these scenarios, and the proposed algorithm has higher efficiency.

## 1. Introduction

The MPPT technique is used to ensure that the PV array always acts supplying the maximum power as possible, because of the nonlinear characteristics of the PV array [1, 2]. Many MPPT techniques have been presented and discussed in the literature [3–7]. And they can be classified as the conventional MPPT techniques and advanced techniques.

The conventional MPPT techniques include perturb and observe (P&O) [6–9], INC [10–13], and incremental resistance (INR) [14]. And they are the most popular algorithms because of their simple structure and easy implementation. However, their duty cycle has an oscillation at the steady state [6], which results in power losses. The advanced techniques, including fuzzy logic [15], neural network [16], and evolutionary computation [17–19], can yield superior performance under the uniform solar irradiance and partially shaded conditions [6]. Nevertheless, they are hard to implement and rely heavily on precise settings of parameters [14, 20].

In the case of the rapid changes of solar irradiation or load resistance, the response of the P&O and INC algorithms with the fixed step size is low. Therefore, the P&O and INC algorithms with a variable-step size are proposed [21, 22]. However, the step size becomes smaller when the operating point is close to the MPP [23].

A few modified algorithms have been introduced to enhance the converging speed during the variation of the solar irradiation level and load. In [24], a novel MPPT technique is introduced that uses the MPP locus proposed in [25] and the short-circuit current, load current, and voltage to track the MPP. The process of determining the short-circuit current and open-circuit voltage results in large power loss and low efficiency. A fast converging algorithm is introduced in [23, 26] that uses the relationship between the load line and the *I*-*V* curve. However, its tracking speed is slightly slow under the increase of solar irradiation. A modified P&O algorithm is introduced in [27] to improve the efficiency, and it uses a dynamic boundary to mitigate the probability of losing the tracking direction. An improved Beta algorithm is proposed in [28] to enhance the tracking speed and eliminate the oscillations at a steady state. In [29], the relationship between the voltage and the current of the MPP and

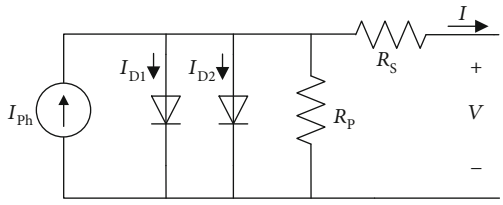


Figure 1: The two-diode model of solar cells.

irradiation level is used to guarantee fast converging speed and negligible oscillations around the MPP. The faster and more robust MPPT technique, which uses a Bode ideal cutoff (BICO) filter in the extremum seeking controller (ESC), is proposed in [30] to achieve a transient rise to the MPP. The quick MPPT technique is introduced in [31], and it can yield good performance under the uniform solar irradiance and partially shaded conditions by using the internal parameters of the PV module.

In this work, a new MPPT technique is proposed to track the MPP directly and also suitable for the fast change of irradiation and load. And it consists of two stages: (1) the computing stage and (2) the regulating stage. The computing stage includes the coarse positioning operation and fine positioning operation, which generates an initial value of the duty cycle according to the characteristics of the DC-DC converter and the characteristics of the $I$-$V$ curve. The duty cycle generated by the computing stage is close to the MPP duty cycle. Thus, this stage enhances the tracking speed. The regulating stage regulates the duty cycle by using a small step size, and it is performed till the set condition is met. And the set condition is introduced in Section 3. This stage improves efficiency by ensuring that the operating point is on the MPP or close to it.

This paper is structured as follows. Following Introduction, Section 2 presents the PV modeling and introduces the PV characteristics under the different solar irradiation levels. Section 3 presents the design of the boost converter, the conventional algorithm, and the new MPPT technique. The simulation results under different scenarios are demonstrated in Section 4, and Section 5 gives the conclusion of the paper.

## 2. PV Modeling and Characteristics

*2.1. Model of PV Panel.* The most popular PV models are the single-diode model and the two-diode model [32]. For the accurate data, the two-diode model in [33] is used in this paper as shown in Figure 1.

The mathematical model of the PV panel can be presented by the following equations [33]:

$$I = I_{ph} - I_{D1}\left[\exp\left(\frac{q(V+IR_s)}{\alpha_1 KTN_S}\right) - 1\right] - I_{D2}\left[\exp\left(\frac{q(V+IR_s)}{\alpha_2 KTN_S}\right) - 1\right] - \left(\frac{V+IR_s}{R_P}\right), \quad (1)$$

Table 1: Main product parameters of the PV module MSX-64.

| PV panel parameters | Values |
|---|---|
| Maximum power, $P_{mmp}$ | 64 W |
| Maximum power point voltage, $V_{mmp}$ | 17.5 V |
| Maximum power point current, $I_{mmp}$ | 3.66 A |
| Short-circuit current, $I_{SC}$ | 4 A |
| Open-circuit voltage, $V_{OC}$ | 21.3 V |
| Voltage/temp. coefficient, $K_V$ | -0.08%/°C |
| Current/temp. coefficient, $K_I$ | 0.003%/°C |
| The number of cells, $N_S$ | 36 |

and the diode saturation current $I_{D1}$ and $I_{D2}$ is given by [33]

$$I_{D1} = I_{D2} = \frac{I_{SC} + K_I \Delta T}{\exp\left(q(V_{OC} + K_V \Delta T)/\alpha_1 KTN_S\right) - 1}. \quad (2)$$

The specifications for the PV module used in this paper are given in Table 1 [34].

*2.2. Characteristic Curves of PV Array.* The PV modules utilized are the MSX-64 configured in a $3 \times 1$ array. When the temperature is 25°C, the $I$-$V$ and $P$-$V$ curves under different solar irradiation levels are shown in Figure 2.

As shown in Figure 2, the PV array current depends heavily on solar irradiation. However, the MPP voltage $V_{mmp}$ increases slowly when the irradiation increases. The markers in Figure 2 are the MPPs under different irradiation levels, and the MPPs can be connected approximately by a straight line (MPP line) [25].

## 3. The New MPPT Technique with Boost Converter

*3.1. Boost Converter Design.* The MPPT system is a DC-DC converter controlled through a strategy (i.e., MPPT technique), and it acts as a power interface between the PV module and the load [1, 35]. There are several DC-DC converters, including buck, boost, buck-boost, SEPIC, and Cúk converters. Among those converters, buck and boost converters both have a simpler structure and higher efficiency. Thus, the boost converter is used in this paper. And the MPPT control system based on the boost converter is shown in Figure 3.

The operation principle of this converter is described by the following equations [36]:

$$V_{out} = V_{PV} M_{(D)}, \quad (3)$$

$$I_{out} = \frac{I_{PV}}{M_{(D)}}, \quad (4)$$

$$V_{out} \times I_{out} = V_{PV} \times I_{PV}, \quad (5)$$

where $M_{(D)} = 1/(1-D)$.

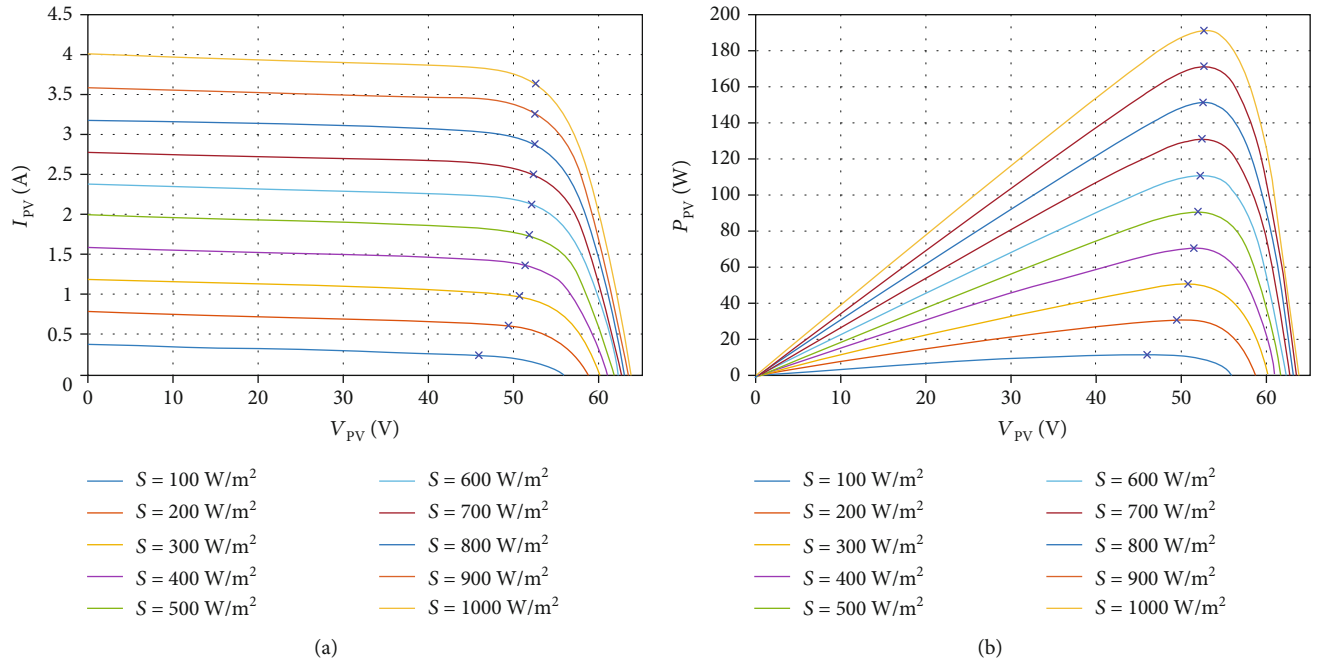


Figure 2: $I$-$V$ and $P$-$V$ curves for different values of solar irradiation: (a) $I$-$V$ curves; (b) $P$-$V$ curves.

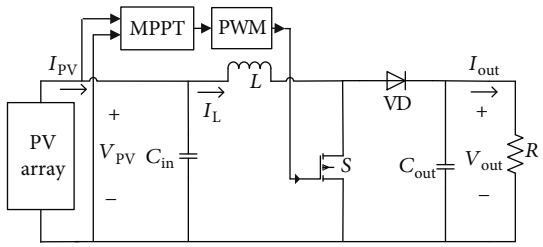


Figure 3: MPPT control system based on the boost converter.

The voltage ripple of input capacitor $C_{in}$ and output capacitor $C_{out}$ in the boost circuit can be computed as [36]

$$\Delta V_{C_{in}} = \frac{D \cdot V_{PV}}{8LC_{in}f_s^2},$$
$$\Delta V_{C_{out}} = \frac{D \cdot V_{out}}{RC_{out}f_s}, \tag{6}$$

and the current ripple of inductor $L$ in the boost circuit also can be computed as [36]

$$\Delta I_L = \frac{DV_{out}}{2Lf_s}, \tag{7}$$

to make the boost converter operate in the continuous conduction mode (CCM). Therefore,

$$L \geq \frac{R}{2f_s} D(1-D)^2. \tag{8}$$

According to [10],

$$\Delta V_{C_{out}} \leq 2\% V_{out},$$
$$\Delta V_{C_{in}} \leq 1\% V_{PV}. \tag{9}$$

Then,

$$C_{in} \geq \frac{D}{0.08Lf_s^2},$$
$$C_{out} \geq \frac{D}{0.02Rf_s}. \tag{10}$$

*3.2. The Conventional INC Algorithm.* The INC algorithm uses the instantaneous conductance of the PV array and the incremental conductance and compares them in order to obtain the MPP [35]. That is to say, it is based on the slope of the PV array power versus voltage curve is zero at the MPP. Therefore, this algorithm can be modeled as follows:

$$\frac{dI}{dV} = -\frac{I}{V} \text{ at MPP}, \tag{11}$$

$$\frac{dI}{dV} > -\frac{I}{V} \text{ on the left side of the MPP}, \tag{12}$$

$$\frac{dI}{dV} < -\frac{I}{V} \text{ on the right side of the MPP}. \tag{13}$$

The flowchart of the INC algorithm is presented in Figure 4 [6]. This algorithm measures the current and voltage of the PV array. If (12) is met, the duty cycle is decreased, and vice versa if (13) is met [10].

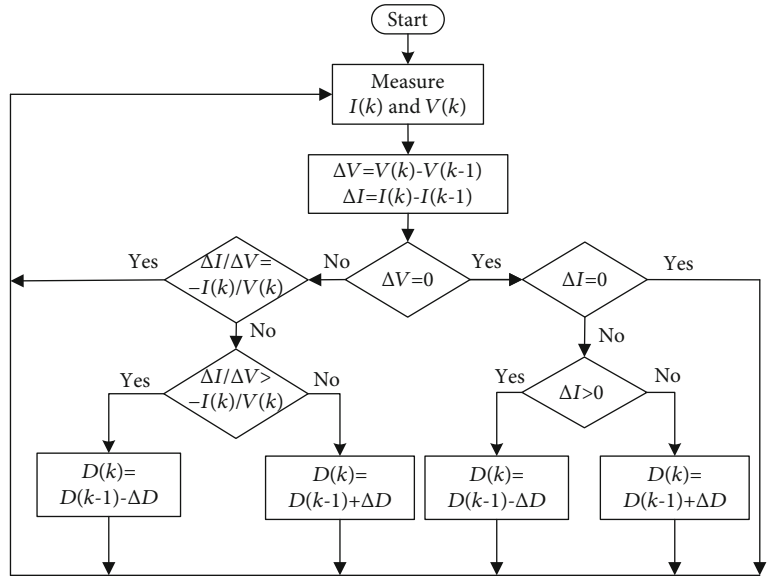


Figure 4: Flowchart of the conventional INC algorithm.

The power drawn from the PV array with a lager step size contributes to faster dynamics but excessive steady state oscillations, resulting in a comparatively low efficiency [22]. The converging speed is low, when this algorithm tracks the MPP with a smaller step size.

*3.3. The New MPPT Technique.* To solve the above problem, a new MPPT algorithm is proposed in this paper. It consists of two stages: (1) the computing stage and (2) the regulating stage. And the computing stage includes the coarse positioning operation and fine positioning operation. An initial value of the duty cycle is generated in the computing stage, according to the characteristics of the DC-DC converter and the characteristics of the *I-V* curve. The regulating stage regulates the duty cycle by using a small step size. So, the regulating stage can improve the efficiency by ensuring that the operating point is on the MPP or close to it. And the computing stage can enhance the response speed.

Substituting $M_{(D)} = 1/(1-D)$, $P_{PV} = V_{PV}I_{PV}$ into (4) and (5), respectively, yields

$$I_{out} = \frac{V_{PV}I_{PV}}{V_{out}} = \sqrt{\frac{P_{PV}I_{out}}{V_{out}}}, \tag{14}$$

$$D = \frac{I_{PV} - I_{out}}{I_{PV}}. \tag{15}$$

According to (14) and (15), if the variable $P_{PV}$ in (14) is the PV maximum power $P_{mpp}$, the variable $D$ obtained by (15) is the MPP duty cycle. The $P_{mpp}$ can be regarded as the product of the short-circuit current $I_{SC}$ and the MPP voltage $V_{mpp}$ in [20], as shown in

$$P_{mpp} = V_{mpp}I_{mpp} \approx V_{mpp}I_{sc}. \tag{16}$$

By substitution of (16) into (14) and (15), we obtain

$$I_{out@mpp} = \sqrt{\frac{V_{mpp}I_{mpp}I_{out}}{V_{out}}} \approx \sqrt{\frac{V_{mpp}I_{SC}I_{out}}{V_{out}}}, \tag{17}$$

$$D = \frac{I_{mpp} - I_{out@mpp}}{I_{mpp}} \approx \frac{I_{SC} - I_{out@mpp}}{I_{SC}}. \tag{18}$$

The $D$ value obtained by (18) is close to the MPP duty cycle. But the variables $V_{mpp}$ and $I_{SC}$ in (17) are unknown. According to the MPP locus in [25], the variable $V_{mpp}$ in (17) can be replaced by the previously tracked MPP voltage. To get the $I_{SC}$ value, a method is introduced in [20] that the switching device of the DC-DC converter is kept ON for a certain period of time. Although an accurate $I_{SC}$ value can be obtained by this method, this process results in large power losses. This paper finds the approximate value for the variable $I_{SC}$ or $I_{mpp}$ in (17) and (18), according to the variation of the operating point during the variation in solar irradiation or load resistance.

*3.3.1. Decrease in Solar Irradiation Level.* When the solar irradiation level is 1000 W/m$^2$, the PV array operates at point B of the load line 2, as shown in Figure 5(a). Then, if the irradiance is decreased from 1000 W/m$^2$ to 400 W/m$^2$, the operating point immediately switches from point B to $B_1$ along the load line 2, because the duty cycle remains unchanged. As presented in Figure 5(a), $I_{B_1} < I_B$, $V_{B_1} < V_{mpp1}$, and the operating current, $I_{B_1}$, is close to the MPP current of 400 W/m$^2$, $I_A$. So,

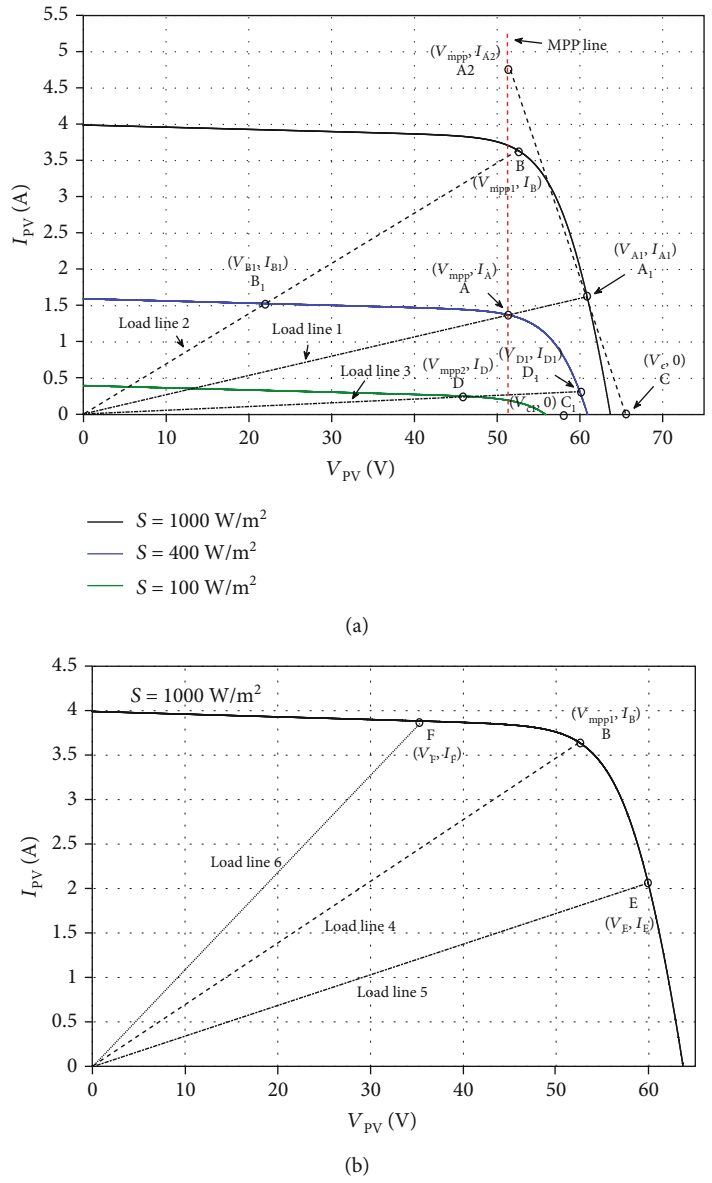


FIGURE 5: The variation in operating point during the variation in solar irradiation or load resistance: (a) the solar irradiation variation; (b) the load resistance variation.

substituting $I_{mpp} \approx I_{B_1}$ and $I_{B_1} = I_{PV}$ into (17) and (18) yields

$$I_{out@mpp} \approx \sqrt{\frac{V_{mpp} I_{B_1} I_{out}}{V_{out}}} = \sqrt{\frac{V_{mpp} I_{PV} I_{out}}{V_{out}}}, \tag{19}$$

$$D = \frac{I_{B_1} - I_{out@mpp}}{I_{B_1}} = \frac{I_{PV} - I_{out@mpp}}{I_{PV}}. \tag{20}$$

*3.3.2. Increase in Solar Irradiation Level.* If the PV array operates at point A in Figure 5(a), the current and voltage of the PV array are $I_A$ and $V_{mpp}$, respectively. Then, if the solar irradiation suddenly increases to 1000 W/m$^2$, the operating point changes from point A to $A_1$ along the load line 1. However, the current of the operating point $A_1$, $I_{A_1}$, is far away from the MPP current of 1000 W/m$^2$, $I_B$. The trigonometry rule in [23] can be used to make the extension line of segment $CA_1$ intersect the MPP line at point $A_2$, as shown in Figure 5(a). It can be found that $|I_{A_2} - I_B| < |I_{A_1} - I_B|$. So, substituting $I_{mpp} \approx I_{A_2}$ into (17) and (18) yields

$$I_{out@mpp} \approx \sqrt{\frac{V_{mpp} I_{A_2} I_{out}}{V_{out}}}, \tag{21}$$

$$D = \frac{I_{A_2} - I_{out@mpp}}{I_{A_2}}. \tag{22}$$

The variable $I_{A_2}$ can be computed as follows [23]:

$$I_{A_2} = \frac{V_{mpp} - V_c}{V_{A_1} - V_c} I_{A_1}, \tag{23}$$

and the variable $V_C$ can be computed as [23]

$$V_C = \frac{V_{mpp}}{0.8}. \tag{24}$$

When the irradiance level is 100 W/m$^2$, the PV array operates at point D of the load line 3, as shown in Figure 5(a). Then, if the irradiance is increased from 100 W/m$^2$ to 400 W/m$^2$, the operating point moves from point D to $D_1$. Substituting $V_{mpp} = V_{mpp2}$ into (24) obtains $V_{C_1} = V_{mpp2}/0.8$, and it is the voltage of point $C_1$. It is found that $V_{C_1} < V_{D_1}$ and $V_{C_1} > V_{mpp2}$. By substituting $V_C = V_{C_1}$, $V_{A_1} = V_{D_1}$, and $V_{mpp} = V_{mpp2}$ into (23), it is obvious that the obtained $I_{A_2}$ is negative. That is to say, the modified INC in [23] is unable to be implemented when the irradiance is increased from 100 W/m$^2$ to 400 W/m$^2$. To ensure $I_{A_2} > 0$, equation (24) need be rewritten as

$$V_C = \begin{cases} V_{mpp}/0.8, & V_{mpp}/0.8 > V_{A_1}, \\ V_{A_1} + n \times V_{AW}, & V_{mpp}/0.8 = V_{A_1}, \\ V_{A_1} + n \times \left(V_{A_1} - V_{mpp}/0.8\right), & V_{mpp}/0.8 < V_{A_1}. \end{cases} \tag{25}$$

*3.3.3. Increase in Load.* When the load resistance is 100 Ω, the PV array operates at point B of the load line 4, as shown in Figure 5(b). Then, if the load resistance is increased from 100 Ω to 200 Ω, the operating point switches from point B to E, and the load line becomes load line 5. It is noteworthy that the *I-V* curve and the MPP both remain unchanged. Therefore, equations (17) and (18) can be rewritten as

$$I_{out@mpp} = \sqrt{\frac{V_{mpp} I_{mpp} I_{out}}{V_{out}}}, \tag{26}$$

$$D = \frac{I_{mpp} - I_{out@mpp}}{I_{mpp}}. \tag{27}$$

*3.3.4. Decrease in Load.* When the PV array operates at point B of the load line 4, if the load resistance is decreased from 100 Ω to 50 Ω, the operating point immediately changes from point B to F, and the load line becomes load line 6, as shown in Figure 5(b). The new MPP can be tracked by using (26) and (27) because the MPP remains unchanged.

The relation between the voltage and current of the PV array and solar irradiation or load resistance is summarized in Table 2.

The flow chart of the proposed algorithm is shown in Figure 6. The variables *flag_inc* and *flag_dec* mean the increase and decrease in the solar irradiation level, respectively. Similarly, when the load resistance is increased and decreased, the variables *flag_load_inc* and *flag_load_dec* are set to 1, respectively. The variable *Flag* is used to indicate that the PV system is operating at the MPP if it is set to 1. Because equation (11) can never be met in practical [17], a permitted error is accepted to detect if the MPP is reached, as shown in equation (28) [11]:

Table 2: Variation in the voltage and current during the variation in solar irradiation or load resistance.

| | Solar irradiation | | Load resistance | |
|---|---|---|---|---|
| | Increase | Decrease | Increase | Decrease |
| $dI$ | + | − | − | + |
| $dV$ | + | − | + | − |

$$\left|\frac{I}{V} + \frac{\Delta I}{\Delta V}\right| < 0.04. \tag{28}$$

Equation (29) is used to improve efficiency by ensuring that the operating point is on the MPP or close to it, as shown as

$$\left|\frac{I}{V} + \frac{\Delta I}{\Delta V}\right| < 0.02. \tag{29}$$

And the duty cycle of the DC-DC converter is regulated by a small step size (i.e., 0.007). That is the regulating stage of the proposed technique. When (28) is met but (29) is not, the regulating stage is performed, as shown in Figure 6(a).

The proposed technique firstly tracks the MPP by using the INC technique as shown in Figure 6(a). When the MPP is tracked (i.e., equation (28) is met.), the MPP voltage and current are stored as $V_{mpp}$ and $I_{mpp}$, respectively. And the variable *Flag* is set to one. If (29) is not met at the next sample cycle, the regulating stage of the proposed technique is performed, and vice versa if (29) is met.

After that, when (28) is not met and *Flag* is one, the proposed technique calls CPO subroutine, as shown is Figure 6(a). The CPO subroutine in Figure 6(b) is the coarse positioning operation of the proposed technique. Then, the variable *Flag* is set to zero, and the variables $V_{out}$ and $I_{out}$ are calculated by using (3) and (4), respectively. Afterward, the variation of solar irradiation or load resistance is detected by using $dI$ and $dV$. Finally, the duty cycle is updated by (21), (22), and (23) if the increase of solar irradiation is detected; the duty cycle is calculated by (19) and (20) if the detection result is the decrease of solar irradiation; otherwise, the duty cycle is updated by using (26) and (27).

At the next sample cycle, the proposed technique calculates $I_{out}$ and $V_{out}$ and calls FPO subroutine, as shown in Figure 6(a). The FPO subroutine in Figure 6(c) is the fine positioning operation. In this subroutine, the duty cycle is updated by different equations under the variation of solar irradiation and load resistance. For the variation of solar irradiation, the equations for the fine positioning operation are

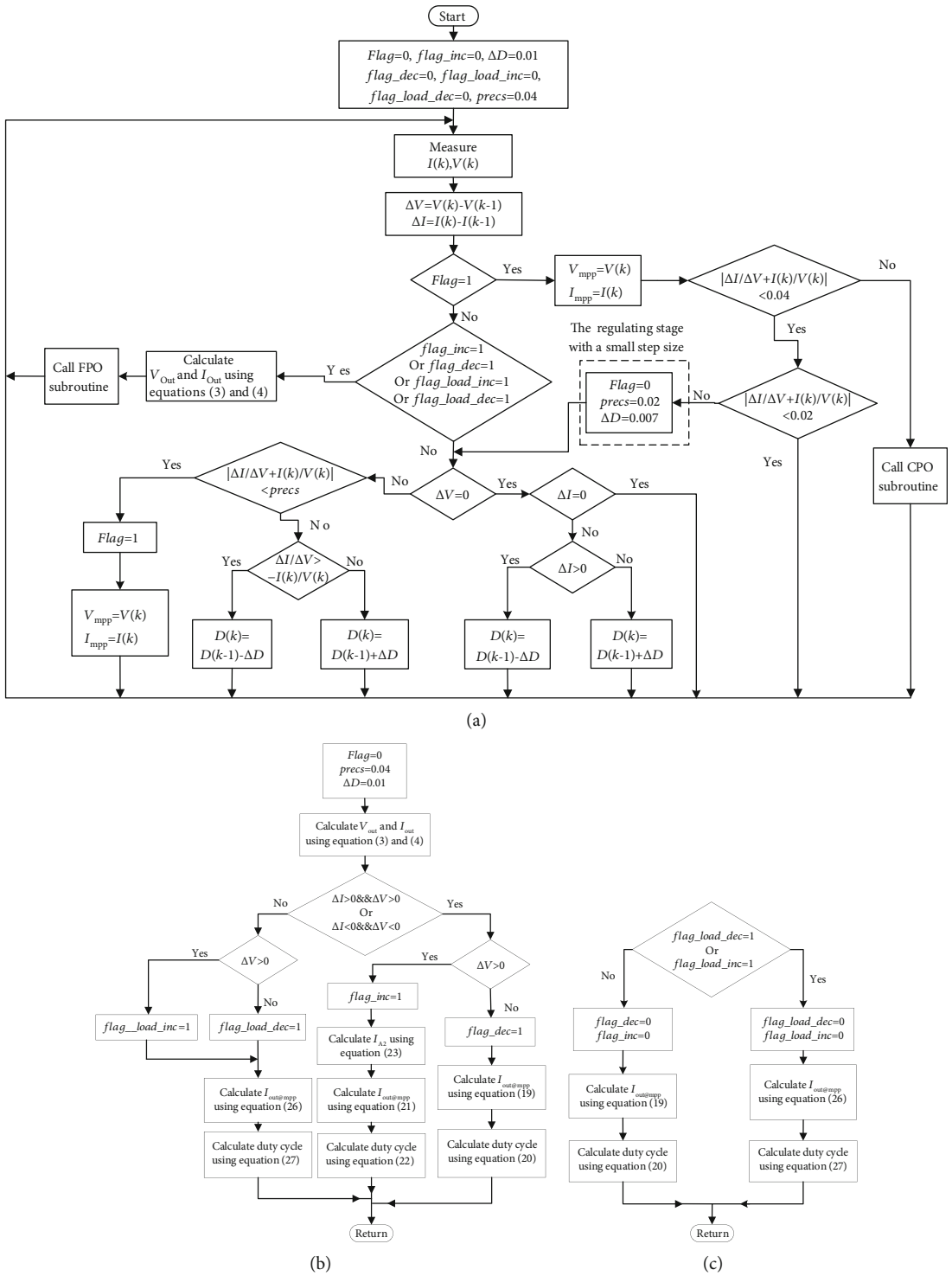


FIGURE 6: Flowchart of the proposed algorithm: (a) main program; (b) CPO subroutine; (c) FPO subroutine.

(19) and (20); otherwise, the equations are (26) and (27). After the FPO subroutine is performed, the operating point is close to the MPP. Thus, the computing stage, including coarse positioning operation and fine positioning operation, can enhance the converging speed. At the next sampling cycle, if (28) is not met, the proposed technique regulates the duty cycle using a big step size (i.e., 0.01). When (28) is met, if (29) is not met, the regulating stage with a small step size (i.e., 0.007) is performed till (29) is met.

## 4. Results and Discussion

Figure 7 shows the MATLAB/Simulink model of the MPPT system. It includes a PV array, boost converter, resistive load,

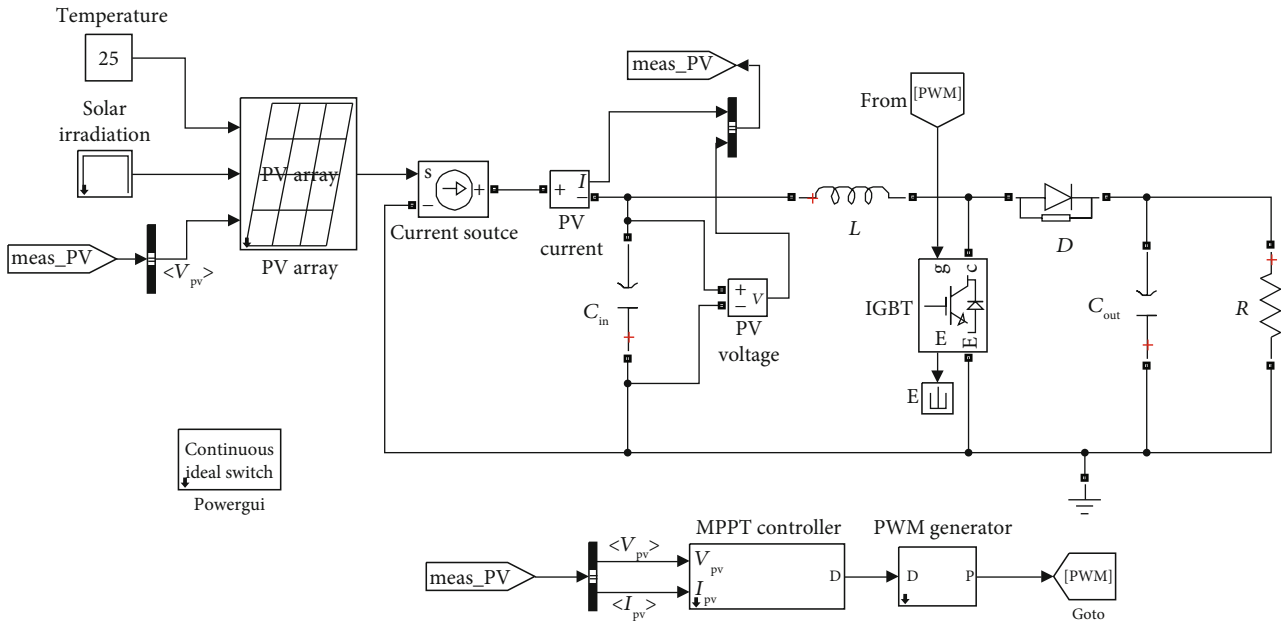


Figure 7: MATLAB simulation model of the MPPT controller and boost converter.

and MPPT controller. The PV modules utilized are the MSX-64 configured in a $3 \times 1$ array. The key specifications of the module are shown in Table 1. The converter is designed for a continuous inductor current mode with the following specifications: $C_{in}$ (PV side) = 470 $\mu$F,$C_{out}$ (boost circuit) = 220 $\mu$F, and $L = 1$ mH. The switching frequency for the IGBT is set to 10 kHz. And a variable resistor is used as the load.

A simulation comparison of the proposed MPPT technique with other techniques, such as conventional INC technique [6], variable-step size INC (VSSINC) [22], and modified INC (MINC) [23], is carried out under different scenarios. The different scenarios include irradiance variation under strong intensity, irradiance variation under weak intensity, and load variation. The sampling time for the MPPT controller is 0.05 s. The step size for conventional INC, MINC, and the proposed technique is 0.01. The maximum step size for VSSINC is 0.04.

*4.1. Irradiance Variation under Strong Intensity.* Figure 8 shows the simulation result for this scenario, where the irradiance level is increased from 400 W/m$^2$ to 1000 W/m$^2$ at $t = 0.799$ s and decreased to 400 W/m$^2$ at $t = 2.799$ s. From $t = 0$ s to $t = 4.8$ s, the load resistance and the temperature are fixed at 80 $\Omega$ and 25°C, respectively.

The conventional INC takes the longest time to track the MPP, as shown in Figure 8. When the irradiance is increased and decreased, it takes 1.45 s and 1.25 s, respectively. And VSSINC and the MINC take less time than conventional INC. When the irradiance is increased to 1000 W/m$^2$, MINC needs shorter time (0.55 s and 11 sampling cycles) to reach the MPP compared to VSSINC (0.7 s and 14 sampling cycles). When the irradiance is decreased to 400 W/m$^2$, MINC also takes shorter time (0.25 s and 5 sampling cycles) to locate the MPP than VSSINC (1.4 s and 28 sampling cycles). During the steady state, the power losses of the MINC and VSSINC are smaller than that of the conventional INC. That is because the conventional INC has a larger oscillation compared to that of VSSINC and MINC at the steady state, as presented in Figure 8(b).

When the irradiance is increased, the proposed technique takes shorter time (0.2 s and 4 sampling cycles) to track the MPP compared to MINC. In contract, when the irradiance is decreased, the proposed technique takes longer time (0.45 s and 9 sampling cycles) to reach the MPP than MINC. However, the overall converging speed of the proposed technique is faster than that of other techniques. The detailed tracking process of the proposed technique is illustrated in Figure 9.

Figure 9 shows the enlarged waveforms of power and duty cycle with the proposed technique when the irradiance is changed and shows the movement of the operating points on the $I - V$ curve. From $t = 0$ s to $t = 0.799$ s, the irradiance level is 400 W/m$^2$. At $t = 0.2$ s, the MPP is tracked as shown in Figure 8(b), and the PV array operates at point A in Figure 9(a). Thus, the variable *Flag* is set to one and the MPP voltage and current are saved as $V_{mpp}$ and $I_{mpp}$, respectively. At $t = 0.799$ s, the irradiance is increased to 1000 W/m$^2$, and the operating point immediately changes from point A to $A_1$ along the load line 1. At $t = 0.8$ s, CPO subroutine is called by the proposed technique because (28) is not met and *Flag* is one. And the CPO subroutine in Figure 6(b) is the coarse positioning operation of the proposed technique. After the CPO subroutine is performed, the duty cycle increases from 33.6% to 50.5%, and the operating point moves from point $A_1$ to $A_3$. At the next sample point $t = 0.85$ s, the FPO subroutine is called by the proposed technique. After that, the duty cycle becomes 54.3%, and the operating point moves to point $A_4$. At the next sampling cycle, the proposed technique regulates the duty cycle using big step size (i.e., 0.01) because (28) is not met. At $t = 1.0$ s,

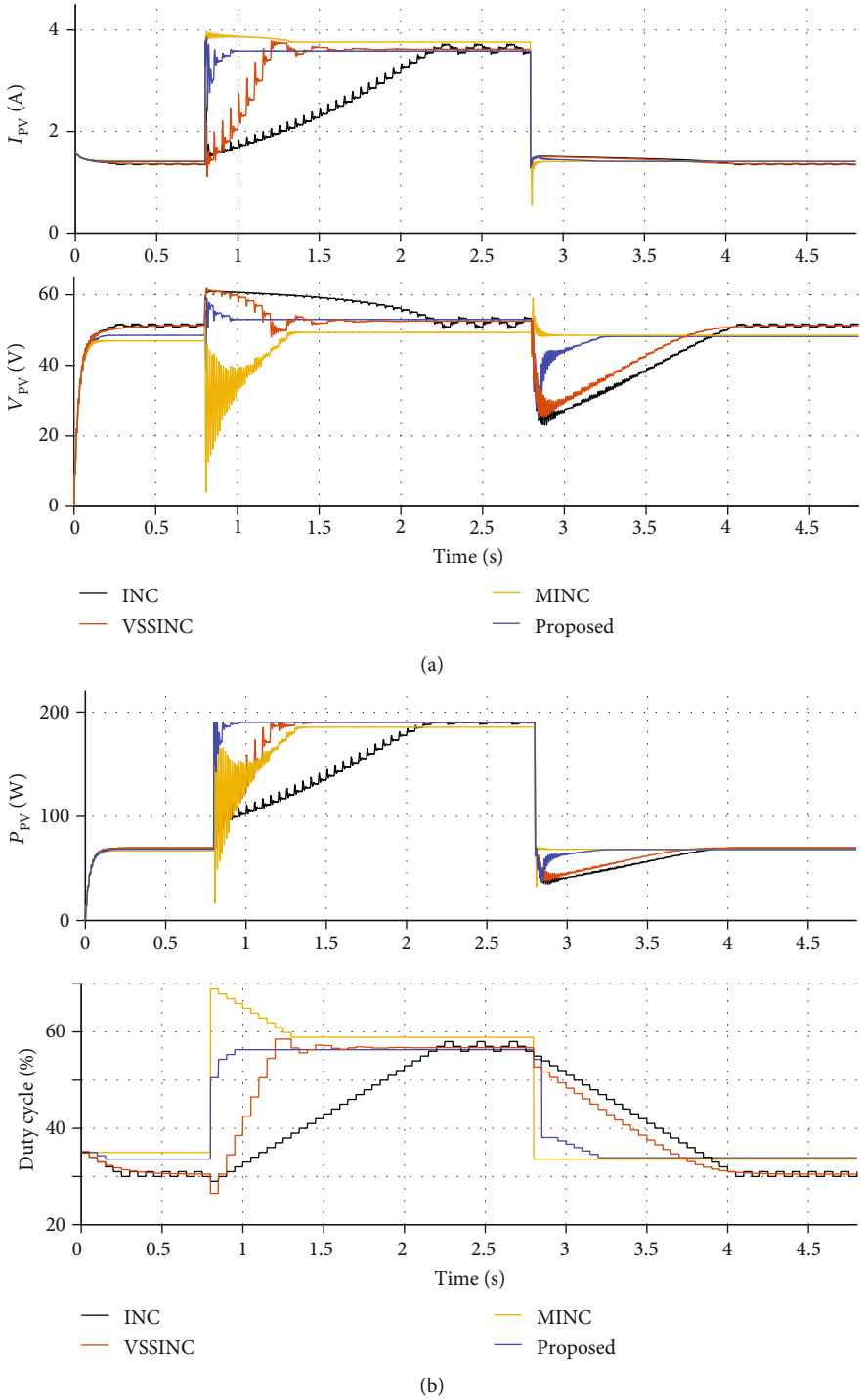


FIGURE 8: Simulation results of the INC, VSSINC, MINC, and the proposed technique for the irradiance variation under strong intensity: (a) current and voltage; (b) power and duty cycle.

(28) is met. The duty cycle is 56.3%, and the operating point is point B. At $t = 1.05$ s, since (29) is met, the regulating operation with a small step size (i.e., 0.007) is not performed.

When the irradiance is decreased to 400 W/m$^2$ at $t = 2.799$ s, a similar process is illustrated in Figure 9(b). At $t = 2.95$ s, the regulating operation with a small step size is performed. The reason is that (28) is met, but (29) is not. After 6 sampling cycles $t = 3.25$ s, (29) is met. The operating point changes from point $B_3$ to A, and the duty cycle is 33.8%. Figure 9(b) shows that the power slowly increases from $t = 2.95$ s to $t = 3.2$ s. That is to say, the regulating operation with a small step size can improve the efficiency.

*4.2. Irradiance Variation under Weak Intensity.* From Section 3, it can be known that MINC cannot be implemented

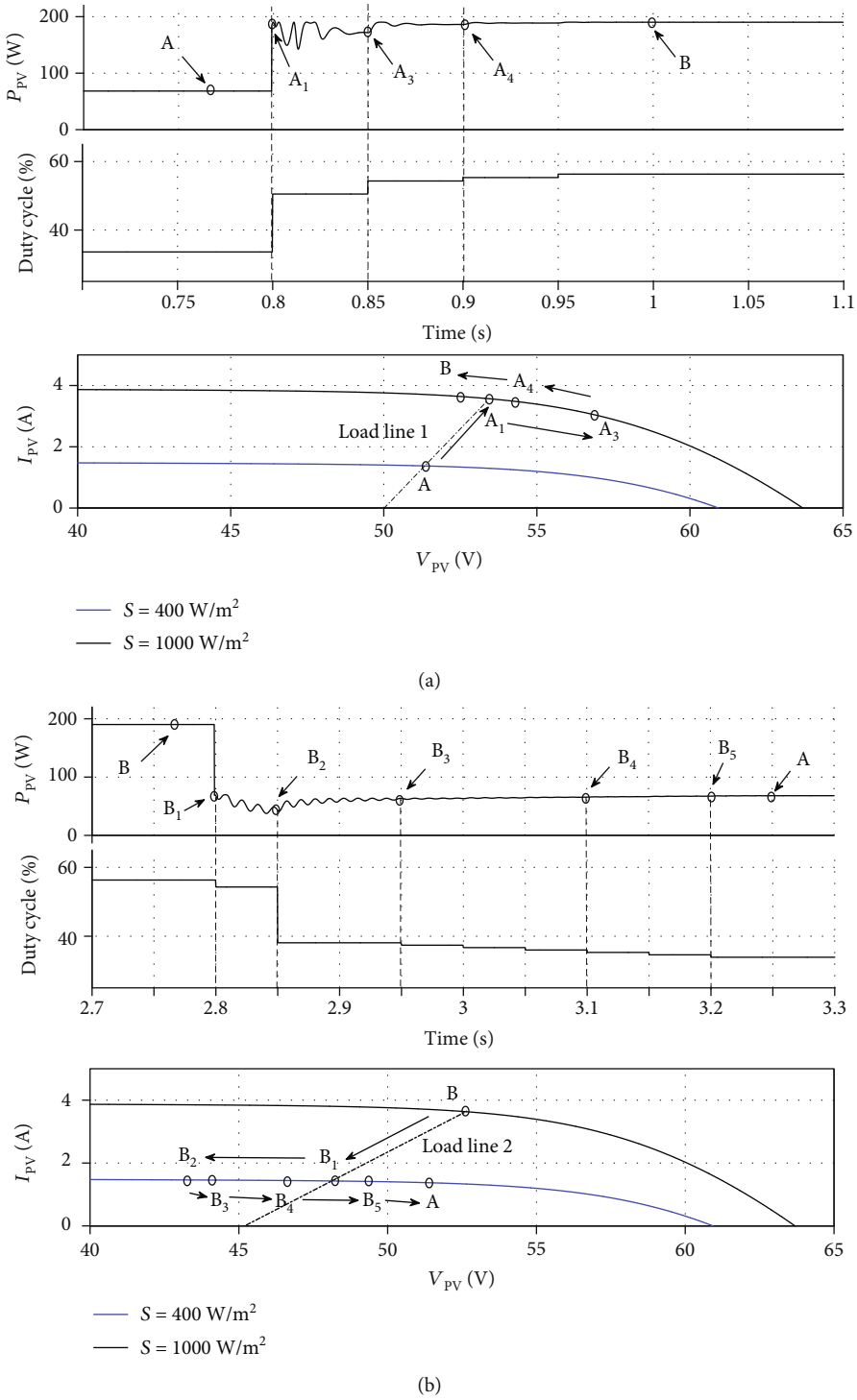


FIGURE 9: Simulation results by using the proposed technique: (a) power, duty cycle, and tracking process when the irradiance is increased; (b) power, duty cycle, and tracking process when the irradiance is decreased.

when the irradiance level is increased from 100 W/m$^2$ to 400 W/m$^2$. That is to say, MINC cannot be carried out for this scenario. Equation (25) is used in the proposed technique when the irradiance is increased from 100 W/m$^2$ to 400 W/m$^2$. And the variables $n$ and $V_{AW}$ in (25) are set to 3 and 4, respectively.

Figure 10 shows the simulation result for this scenario. At $t = 1.985$ s, the irradiance level is increased from 100 W/m$^2$ to 400 W/m$^2$. And the irradiance level is decreased to 100 W/m$^2$ at $t = 4.96$ s. During this period, the load resistance is fixed at 300 Ω, and the temperature is fixed at 25°C.

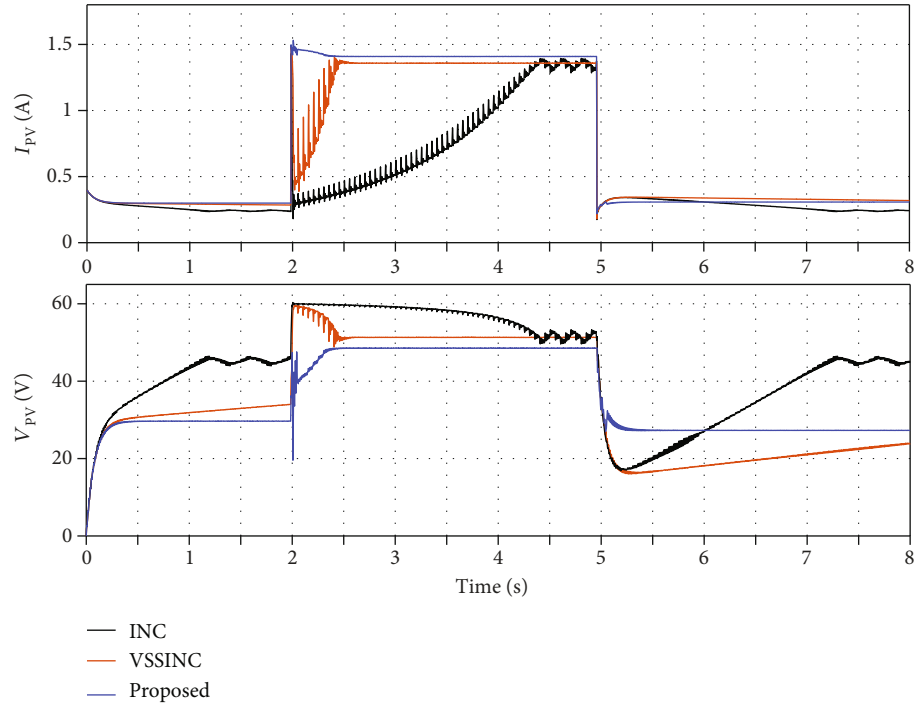


(a)

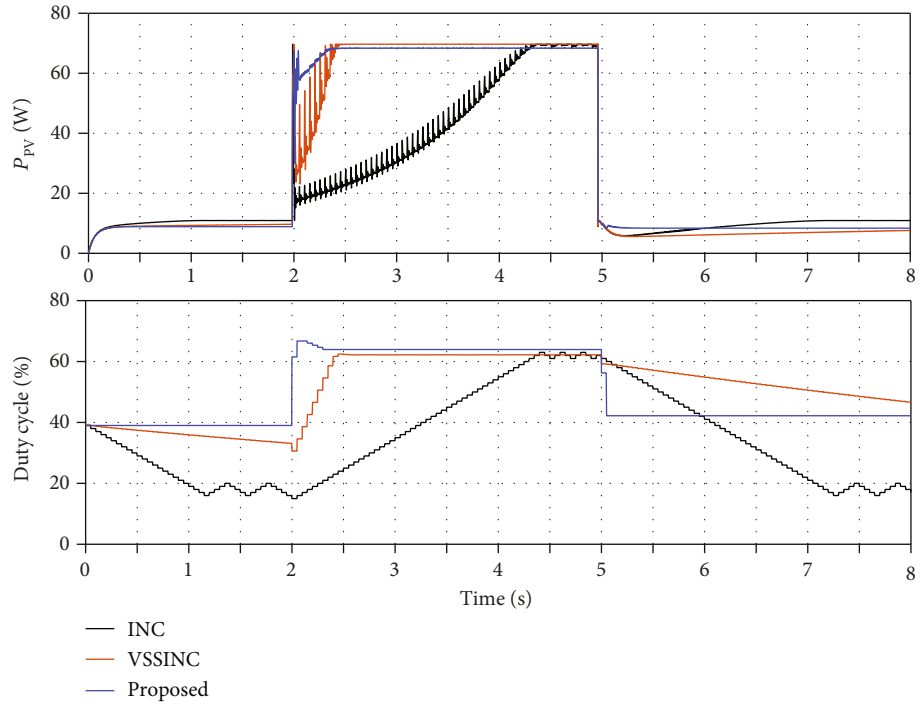


(b)

Figure 10: Simulation results of the INC, VSSINC, MINC, and the proposed technique for the irradiance variation under weak intensity: (a) current and voltage; (b) power and duty cycle.

When the irradiance is increased to 400 W/m$^2$, the proposed technique is the fastest technique which takes 0.45 s to reach the MPP. The conventional INC is the slowest one, and it takes 2.2 s. When the irradiance is decreased from 400 W/m$^2$ to 100 W/m$^2$, the proposed technique is the fastest technique among these techniques, which takes 0.15 s. VSSINC cannot track the MPP in 3 s, since $dP/dV$ is very small when the irradiance level is 100 W/m$^2$. That is to say, the step size of VSSINC is very small, and it results in slow tracking speed. Therefore, VSSINC is the slowest

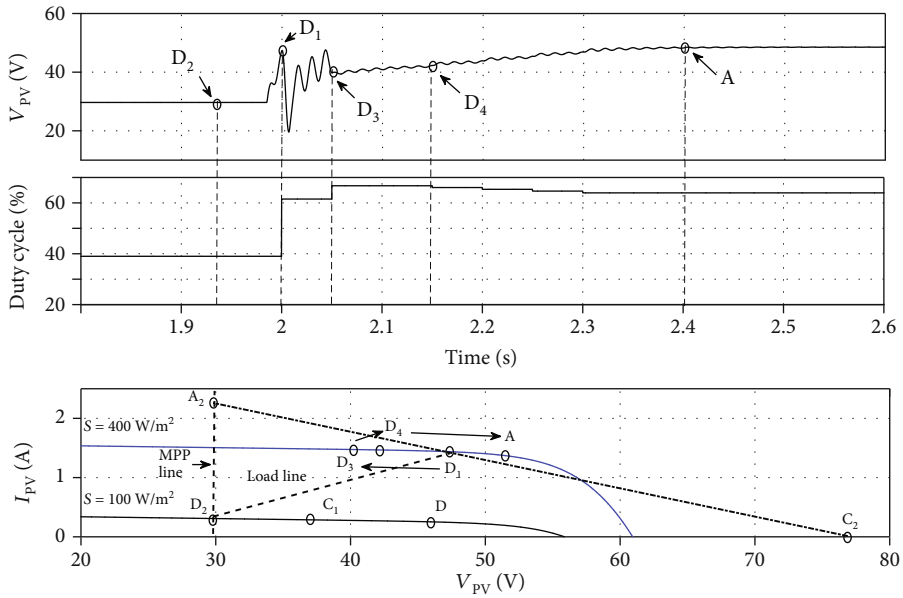


Figure 11: The process of the proposed algorithm when the irradiance is increased to 400 W/m$^2$.

one when the irradiance is decreased. Figure 11 illustrates the detailed process of the proposed technique for the irradiance rising transient.

Figure 11 shows the enlarged waveforms of voltage and duty cycle with the proposed technique when the irradiance is increased to 400 W/m$^2$ and shows the movement of the corresponding operating points on the $I-V$ curve. From $t = 0$ s to $t = 1.985$ s, the irradiance level is 100 W/m$^2$. At $t = 0.3$ s, (29) is met, and the operating point becomes point $D_2$. But the tracked MPPT (i.e., point $D_2$) is not the MPP of 100 W/m$^2$, point D. That is because the slope of the $P$-$V$ curve ($dP/dV$) is small when the solar irradiation is 100 W/m$^2$, which leads to (29) being easily met. At $t = 1.985$ s, the irradiance is increased to 400 W/m$^2$, and the operating point switches from point $D_2$ to $D_1$ along the load line. At the next sampling point $t = 2$ s, the CPO subroutine is called. At that time, $V_{mpp}$ is equal to the voltage of point $D_2$, $V_{D_2}$ (29.67 V). Thus, $V_{mpp}/0.8$ (37.09 V) is the voltage of point $C_1$ in Figure 11. And the voltage of point $D_1$, $V_{D_1}$, is 47.37 V. By substituting $V_{mpp} = 29.67$ V, $V_C = 37.09$ V, and $V_{A_1} = V_{D_1}$ into (23), it is obvious that the obtained $I_{A_2}$ is negative. The reason is $(V_{mpp}/0.8) < V_{D_1}$. $V_C$ is equal to 78.21 V after equation (25) is used. And 78.21 V is the voltage of point $C_2$. Substituting $V_{mpp}$, $V_C = 78.21$ V, and $V_{A_1} = V_{D_1}$ into (23) yields $I_{A_2} = 1.57$ A. After equations (21) and (22) are performed, the duty cycle becomes 61.5%. So, the operating point changes from point $D_1$ to $D_3$. After the FPO subroutine and the regulating stage with a small step size are performed, the PV array operates at point A.

*4.3. Load Variation Condition.* Figure 12 presents the simulation results for this scenario: the load resistance is increased from 100 Ω to 200 Ω at $t = 0.795$ s and then decreased to 100 Ω at $t = 2.795$ s. From $t = 0$ s to $t = 4.8$ s, the irradiance level is kept constant at 500 W/m$^2$, and the temperature is fixed at 25°C.

When the load resistance is increased, MINC takes shorter time (0.3 s and 6 sampling cycles) to reach the MPP compared to the proposed technique (0.4 s and 8 sampling cycles). In contrast, when the load resistance is decreased, the proposed technique takes shorter time (0.25 s and 5 sampling cycles) to locate the MPP than MINC (0.4 s and 8 sampling cycles). But the proposed technique is the fastest technique in terms of the overall converging speed.

The conventional INC is the slowest one, which takes 0.75 s and 0.85 s, respectively. Under the falling load transients, the MPP tracked by MINC is not the MPP of 500 W/m$^2$, as shown in Figure 12(b). And it results in low efficiency and large power losses.

*4.4. One-Day Irradiance Profile.* For the one-day efficiency, the daily (12-hour) irradiance profile of August 23, 2019, in Nanchang City, China, is considered. Figures 13 and 14 present the simulation results for this scenario, where the solar irradiation varies between every 5 min. During the period, the load resistance is kept constant at 300 Ω, and the temperature is fixed at 25°C.

It is obvious that the conventional INC has large steady state oscillations, as shown in Figures 13(a) and 14. Figures 13(b) and 14 show that the VSSINC has small steady state oscillations. When the solar irradiation is increased, the duty cycle should be decreased, but due to the inaccurate response, the duty cycle is decreased [11]. When the solar irradiation suddenly changes, the duty cycle is suddenly decreased by a big step size, which is equal to $N \times |dP/dV|$ or the maximum step size 0.04. And it causes a sudden drop in the current and power and also causes the voltage to suddenly increase, as shown in Figures 13(b) and 14.

It can be found that the voltage decreases from 9:00 as shown in Figure 13(c), because the MINC tracks the wrong

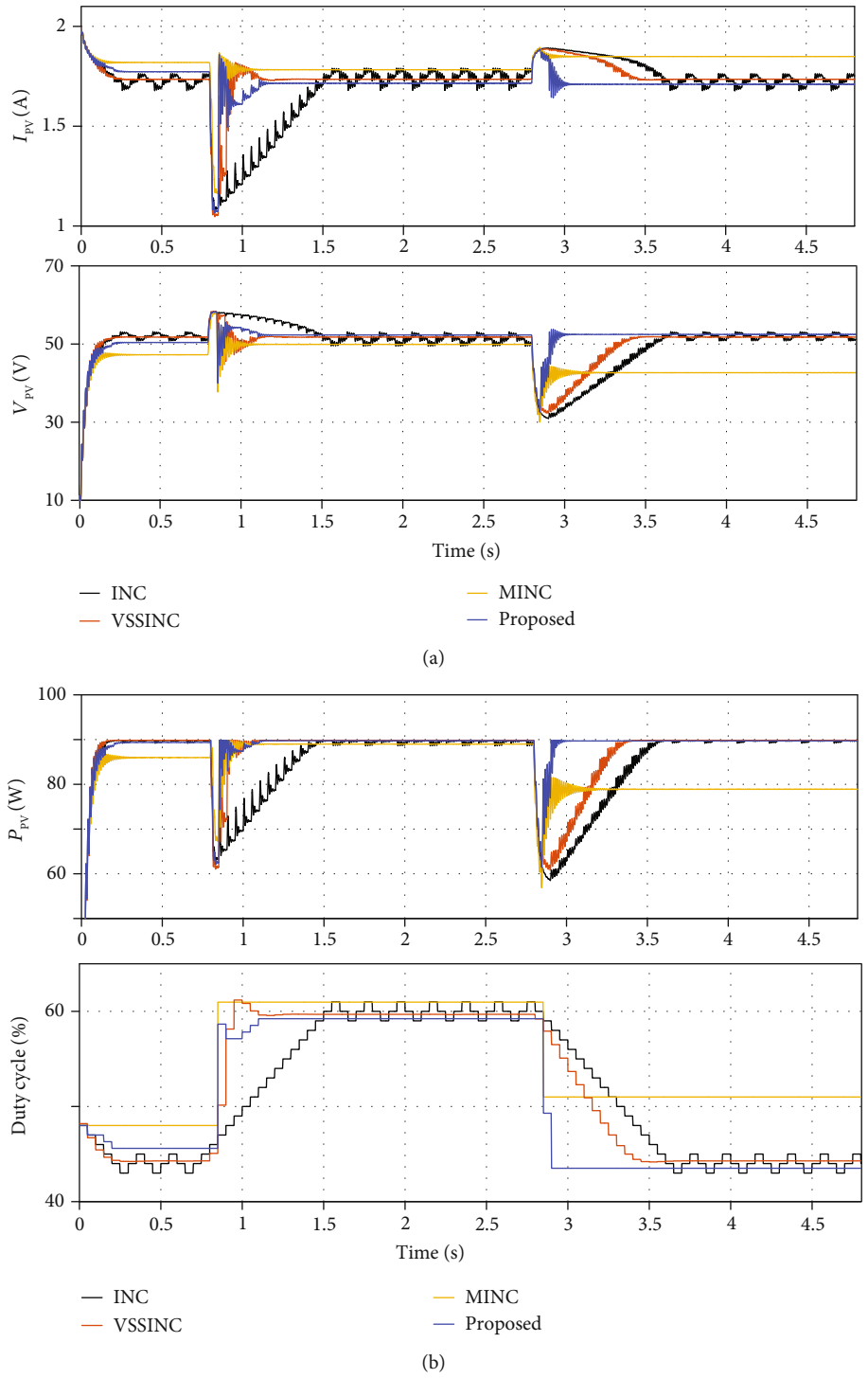


Figure 12: Simulation results of the INC, VSSINC, MINC, and the proposed technique for the load variation condition: (a) current and voltage; (b) power and duty cycle.

MPP and $|dP/dV| < 0.06$ is met. And it results in large power losses. As presented in Figure 13(d), the proposed technique has neglected steady state oscillations.

The tracked power of the proposed technique is less than that of the conventional INC and VSSINC when the solar irradiation is small, as shown in images 1 and 3. That is because the slope of the $P$-$V$ curve ($dP/dV$) is small when the solar irradiation is small, which leads to (29) being easily met. Image 2 shows that the tracked power of the proposed technique is higher than that of the other techniques.

*4.5. Evaluation.* Tables 3 and 4 show the comparison results of the proposed technique with other techniques. And the

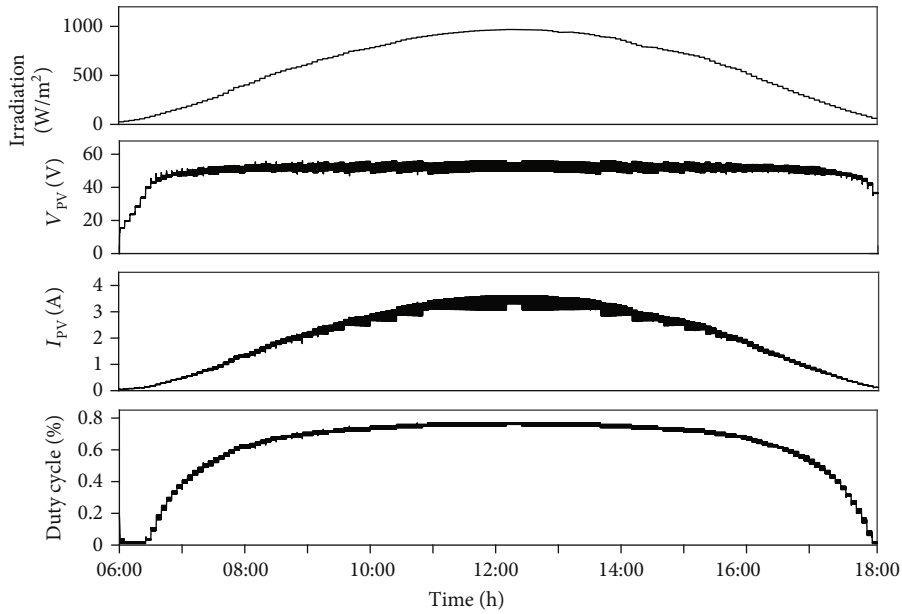


(a)

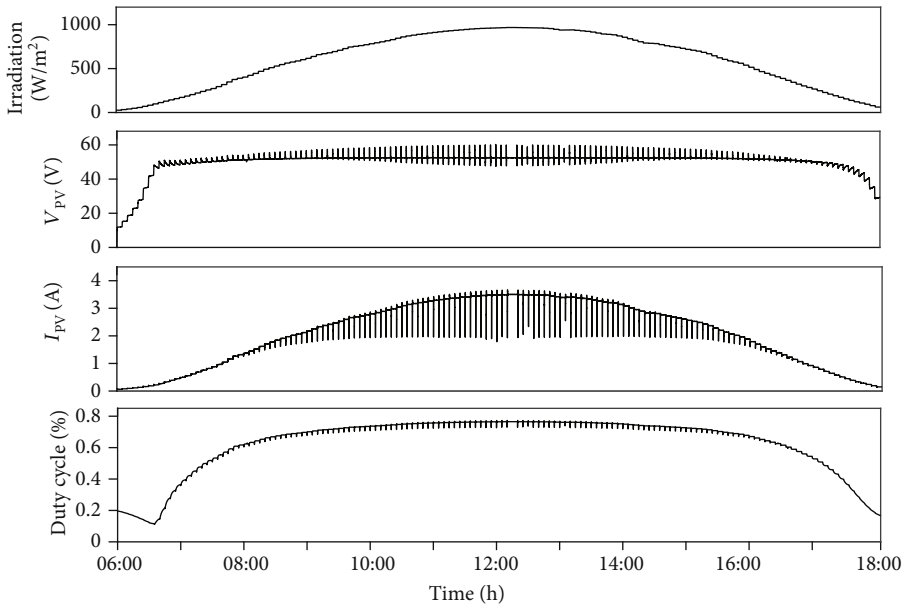


(b)

Figure 13: Continued.

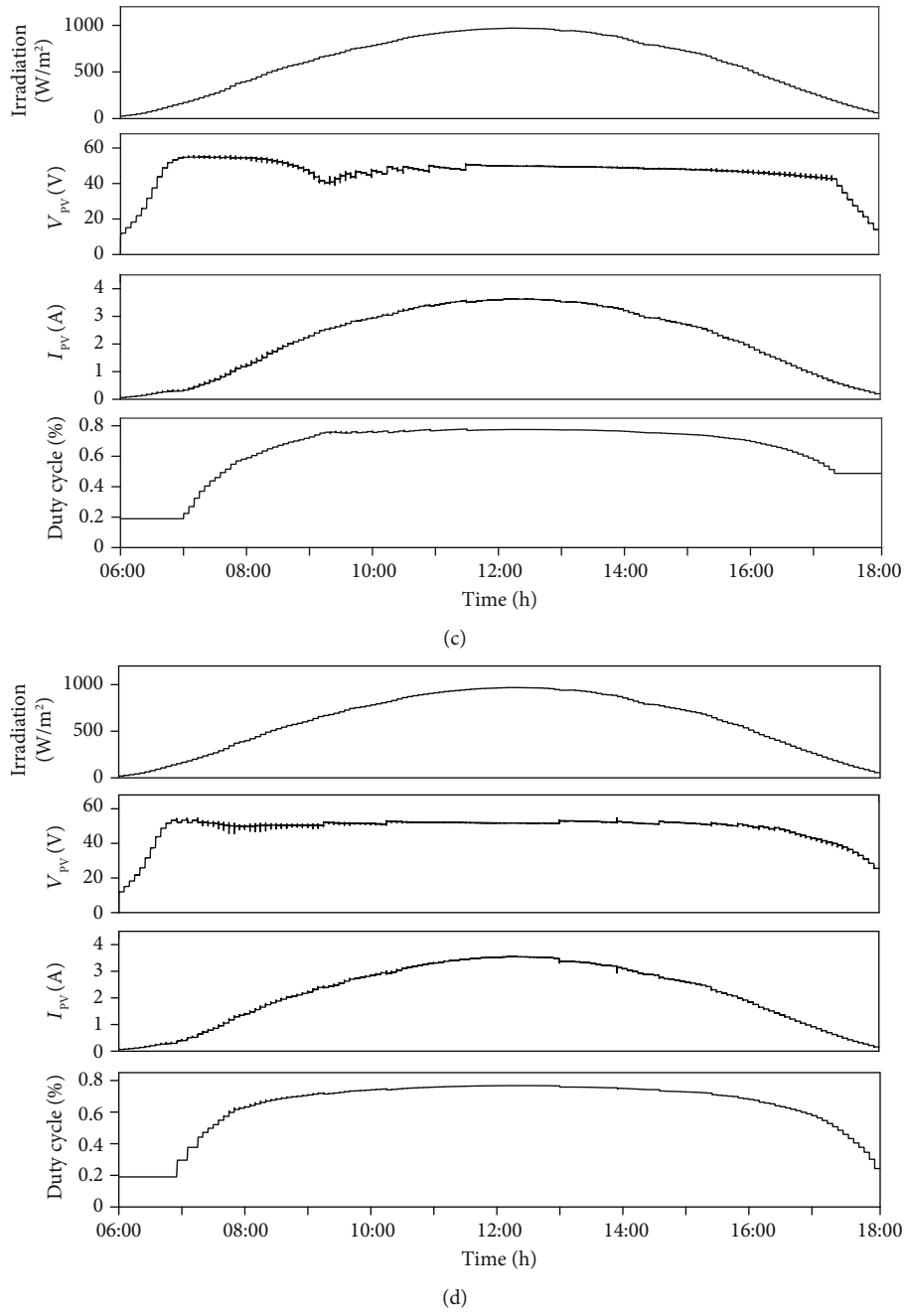


Figure 13: Simulation results of the INC, VSSINC, MINC, and the proposed technique for the one-day irradiance profile: (a) INC; (b) VSSINC; (c) MINC; (d) the proposed technique.

comparison results show the superior performance of the proposed algorithm over other techniques. Here, the tracking power loss $P_{\text{loss}}$ and tracking efficiency $T_{\text{eff}}$ are defined as (30) [28]and (31) [12], respectively:

$$P_{\text{loss}} = \frac{\sum P_{\text{TA}}(t_{\text{track}}) - \sum P_{\text{MPPT}}(t_{\text{track}})}{\sum P_{\text{TA}}(t_{\text{track}})}, \tag{30}$$

$$T_{\text{eff}} = \frac{\int_0^{t_{\text{ts}}} P_{\text{MPPT}}}{\int_0^{t_{\text{ts}}} P_{\text{TA}}} \times 100\%. \tag{31}$$

It is found that the tracking speed of the proposed technique is 4.1 times, 3.2 times, and 1.2 times faster than the conventional INC, VSSINC, and MINC, respectively, for the irradiance variation under strong intensity, as presented in Table 3. The tracking power loss with the proposed technique is less than other techniques, and the efficiency is also higher than other techniques, under this scenario.

For the irradiance variation under weak intensity, the response speed of the proposed technique is 7.3 times and 5.8 times faster than the conventional INC and VSSINC, respectively. The tracking power loss with the proposed technique is less than that of the conventional INC and VSSINC.

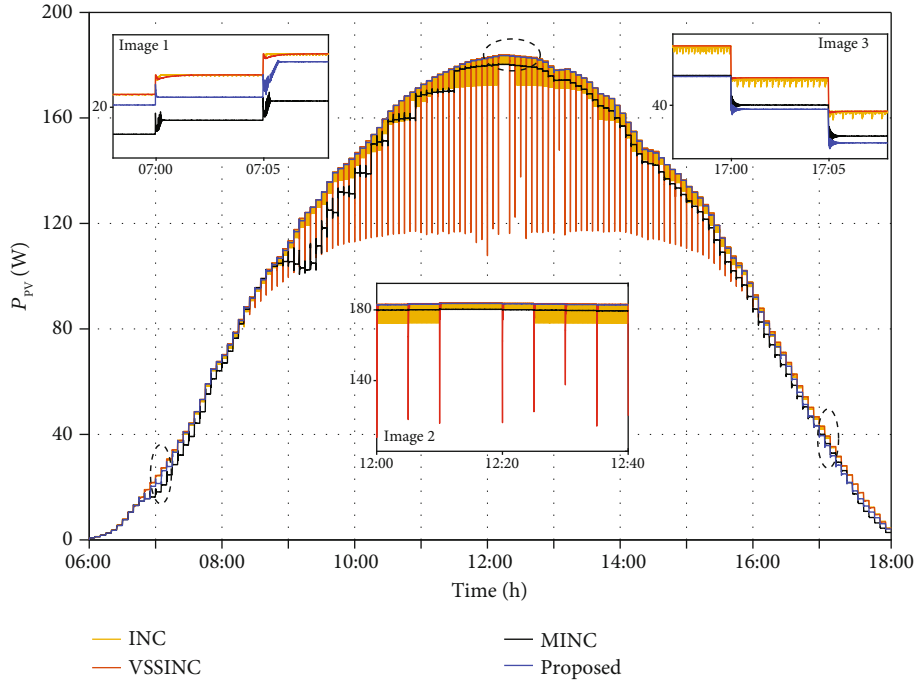


Figure 14: Power waveforms of the INC, VSSINC, MINC, and the proposed technique.

Table 3: Tracking time and power loss comparison of the proposed technique with other techniques.

| Scenario | | Tracking time (s) | | | | Tracking power loss (%) | | | |
|---|---|---|---|---|---|---|---|---|---|
| | | INC | VSSINC | MINC | Proposed | INC | VSSINC | MINC | Proposed |
| Irradiance variation | Strong intensity | 1.35 | 1.05 | 0.4 | 0.33 | 23.30 | 16.01 | 14.33 | 6.59 |
| | Weak intensity | 2.2 | 1.75 | | 0.3 | 33.77 | 33.22 | | 13.18 |
| Load variation | | 0.8 | 0.5 | 0.35 | 0.33 | 14.85 | 10.56 | 10.38 | 6.01 |

Table 4: Efficiency and steady state oscillation comparison of the proposed technique with other techniques.

| Scenario | | Efficiency (%) | | | | Steady state oscillation | | | |
|---|---|---|---|---|---|---|---|---|---|
| | | INC | VSSINC | MINC | Proposed | INC | VSSINC | MINC | Proposed |
| Irradiance variation | Strong intensity | 83.47 | 91.51 | 93.84 | 97.67 | Large | Small | Neglected | Neglected |
| | Weak intensity | 72.83 | 77.10 | | 86.68 | Large | Small | | Neglected |
| Load variation | | 93.36 | 96.86 | 92.71 | 98.91 | Large | Small | Neglected | Neglected |
| One-day profile | | 96.12 | 96.31 | 90.12 | 97.85 | Large | Small | Neglected | Neglected |

And the efficiency is increased by 13.85% and 9.58% in comparison with the conventional INC and VSSINC, respectively, under this scenario.

The average tracking time required by the conventional INC, VSSINC, and MINC under the load variation is 0.8 s, 0.5 s, and 0.35 s, respectively, but the proposed technique requires 0.33 s. The tracking power loss is decreased by 8.84%, 4.55%, and 4.37% in comparison with the conventional INC, VSSINC, and MINC, respectively, during the load variation. And the efficiency is also higher than other techniques.

The efficiency is increased by 1.73%, 1.54%, and 7.73% in comparison with the conventional INC, VSSINC, and MINC, respectively, under the one-day profile scenario.

The steady state oscillation of the proposed technique is neglected because (28) is used. And thanks to (29), the efficiency of the proposed technique is improved. The conventional INC has a large steady state oscillation. That is because the duty cycle has an oscillation at the steady state. In terms of overall efficiency, the highest is the proposed technique at 95.28%, followed by the MINC and VSSINC,

which is 92.22% and 90.45%, respectively, and the lowest is the conventional INC, which is only 86.45%.

## 5. Conclusions

In this paper, a novel MPPT technique is proposed. It includes two stages: the computing stage to enhance the response speed and the regulating stage to improve the tracking efficiency. Various scenarios are analysed, including the irradiance variation, the load variation, and the one-day irradiance profile. The results show that the overall tracking speed of the proposed technique is 4.6 times, 3.5 times, and 1.1 times faster than that of the conventional INC, VSSINC, and MINC, respectively. In addition, the one-day performance shows that the proposed technique yields the highest efficiency compared to other techniques. From the hardware point of view, the proposed technique is simple. Moreover, this technique can be more improved and implemented in a low-cost microcontroller.

## Abbreviations

MPPT: Maximum power point tracking
MPP: Maximum power point
PV: Photovoltaic
P&O: Perturb and observe
INC: Incremental conductance
INR: Incremental resistance
BICO: Ode ideal cutoff
ESC: Extremum seeking controller
STC: Standard test conditions
CCM: Continuous conduction mode
VSSINC: Variable-step size INC in [22]
MINC: Modified INC in [23].

*Nomenclature*

$I_{D1}$: The reverse saturation currents of diode 1 (A)
$I_{D2}$: The reverse saturation currents of diode 2 (A)
$I_{ph}$: PV array photocurrent (A)
$q$: Electron charge (C)
$K$: Boltzmann constant ($J \cdot K^{-1}$)
$T$: Junction temperature (K)
$N_S$: The number of cells
$R_s$: Series resistance ($\Omega$)
$R_P$: Parallel resistance ($\Omega$)
$I_{SC}$: Short-circuit current (A)
$V_{OC}$: Open-circuit voltage (V)
$K_I$: Short-circuit current coefficient (%/°C)
$K_V$: Temperature coefficient of the voltage (%/°C)
$D$: Duty cycle (%)
$I_{PV}$: Output current of the PV array (A)
$V_{PV}$: Output voltage of the PV array (V)
$I_{out}$: Output current of the boost converter (A)
$V_{out}$: Output voltage of the boost converter (V)
$f_s$: Switching frequency (Hz)
$\Delta V_{C_{in}}$: Input voltage ripple of the boost converter (V)
$\Delta V_{C_{out}}$: Output voltage ripple of the boost converter (V)
$\Delta I_L$: Inductor current ripple (A)
$R$: The load ($\Omega$)
$P_{PV}$: Output power of the PV array (W)
$V_{mmp}$: Maximum power point voltage (V)
$I_{mmp}$: Maximum power point current (A)
$n$: The scaling factor
$V_{AW}$: The allowable voltage (V)
$P_{TA}$: The theoretical available power of PV (W)
$P_{MPPT}$: The PV output power using different MPPT techniques (W)
$t_{track}$: The total tracking time required by the different techniques to reach the MPP
$t_{ts}$: The working time under the different cases
$I_{out@mpp}$: Output current of the boost converter at the MPP (A).

*Greek Letters*

$\alpha_1$: Diode 2's ideality factor
$\alpha_2$: Diode 1's ideality factor.

## Data Availability

The data used to support the findings of this study have not been made available because it is confidential.

## Conflicts of Interest

The authors declare that they have no conflicts of interest.

## Acknowledgments

The authors gratefully acknowledge the financial support provided by the National Natural Science Foundation of China (51567019) and the Science and Technology Support Program of Jiangxi Province, China (20142BBE50002).

## References

[1] R. F. Coelho, F. Concer, and D. C. Martins, "A study of the basic DC-DC converters applied in maximum power point tracking," in *2009 Brazilian Power Electronics Conference*, pp. 673–678, Bonito-Mato Grosso do Sul, Brazil, 2009.

[2] Y. H. Ji, D. Y. Jung, J. G. Kim, J. H. Kim, T. W. Lee, and C. Y. Won, "A real maximum power point tracking method for mismatching compensation in PV array under partially shaded conditions," *IEEE Transactions on Power Electronics*, vol. 26, no. 4, pp. 1001–1009, 2011.

[3] M. Balato, L. Costanzo, P. Marino, G. Rubino, L. Rubino, and M. Vitelli, "Modified TEODI MPPT technique: theoretical analysis and experimental validation in uniform and mismatching conditions," *IEEE Journal of Photovoltaics*, vol. 7, no. 2, pp. 604–613, 2017.

[4] L. Costanzo and M. Vitelli, "A novel MPPT technique for single stage grid-connected PV systems: T4S," *Energies*, vol. 12, no. 23, p. 4501, 2019.

[5] N. Femia, G. Petrone, G. Spagnuolo, and M. Vitelli, "Optimization of perturb and observe maximum power point tracking method," *IEEE Transactions on Power Electronics*, vol. 20, no. 4, pp. 963–973, 2005.

[6] M. F. N. Tajuddin, M. S. Arif, S. M. Ayob, and Z. Salam, "Perturbative methods for maximum power point tracking

(MPPT) of photovoltaic (PV) systems: a review," *International Journal of Energy Research*, vol. 39, no. 9, pp. 1153–1178, 2015.

[7] Z. Salam, J. Ahmed, and B. S. Merugu, "The application of soft computing methods for MPPT of PV system: a technological and status review," *Applied Energy*, vol. 107, pp. 135–148, 2013.

[8] T. Esram and P. L. Chapman, "Comparison of photovoltaic array maximum power point tracking techniques," *IEEE Transactions on Energy Conversion*, vol. 22, no. 2, pp. 439–449, 2007.

[9] M. A. G. de Brito, L. Galotto, L. P. Sampaio, G. D. E. Melo, and C. A. Canesin, "Evaluation of the main MPPT techniques for photovoltaic applications," *IEEE Transactions on Industrial Electronics*, vol. 60, no. 3, pp. 1156–1167, 2013.

[10] S. Motahhir, A. El Ghzizal, S. Sebti, and A. Derouich, "Modeling of photovoltaic system with modified incremental conductance algorithm for fast changes of irradiance," *International Journal of Photoenergy*, vol. 2018, Article ID 3286479, 13 pages, 2018.

[11] K. S. Tey and S. Mekhilef, "Modified incremental conductance MPPT algorithm to mitigate inaccurate responses under fast-changing solar irradiation level," *Solar Energy*, vol. 101, pp. 333–342, 2014.

[12] A. Belkaid, I. Colakc, and O. Isik, "Photovoltaic maximum power point tracking under fast varying of solar radiation," *Applied Energy*, vol. 179, pp. 523–530, 2016.

[13] S. Motahhir, A. El Hammoumi, and A. El Ghzizal, "Photovoltaic system with quantitative comparative between an improved MPPT and existing INC and P&O methods under fast varying of solar irradiation," *Energy Reports*, vol. 4, pp. 341–350, 2018.

[14] Q. Mei, M. W. Shan, L. Y. Liu, and J. M. Guerrero, "A novel improved variable step-size incremental-resistance MPPT method for PV systems," *IEEE Transactions on Industrial Electronics*, vol. 58, no. 6, pp. 2427–2434, 2011.

[15] A. El Khateb, N. Abd Rahim, J. Selvaraj, and M. N. Uddin, "Fuzzy-logic-controller-based SEPIC converter for maximum power point tracking," *IEEE Transactions on Industry Applications*, vol. 50, no. 4, pp. 2349–2358, 2014.

[16] Y. H. Liu, C. L. Liu, J. W. Huang, and J. H. Chen, "Neural-network-based maximum power point tracking methods for photovoltaic systems operating under fast changing environments," *Solar Energy*, vol. 89, pp. 42–53, 2013.

[17] M. F. N. Tajuddin, S. M. Ayob, Z. Salam, and M. S. Saad, "Evolutionary based maximum power point tracking technique using differential evolution algorithm," *Energy and Buildings*, vol. 67, pp. 245–252, 2013.

[18] K. Ishaque and Z. Salam, "A deterministic particle swarm optimization maximum power point tracker for photovoltaic system under partial shading condition," *IEEE Transactions on Industrial Electronics*, vol. 60, no. 8, pp. 3195–3206, 2013.

[19] M. Seyedmahmoudian, T. K. Soon, E. Jamei et al., "Maximum power point tracking for photovoltaic systems under partial shading conditions using bat algorithm," *Sustainability*, vol. 10, no. 5, pp. 1347–1362, 2018.

[20] K. S. Tey and S. Mekhilef, "Modified incremental conductance algorithm for photovoltaic system under partial shading conditions and load variation," *IEEE Transactions on Industrial Electronics*, vol. 61, no. 10, pp. 5384–5392, 2014.

[21] F. A. O. Aashoor and F. V. P. Robinson, "A variable step size perturb and observe algorithm for photovoltaic maximum power point tracking," in *2012 47th International Universities Power Engineering Conference (UPEC)*, pp. 1–6, London, UK, September 2012.

[22] F. Liu, S. Duan, F. Liu, B. Liu, and Y. Kang, "A variable step size INC MPPT method for PV systems," *IEEE Transactions on Industrial Electronics*, vol. 55, no. 7, pp. 2622–2628, 2008.

[23] T. K. Soon and S. Mekhilef, "A fast-converging MPPT technique for photovoltaic system under fast-varying solar irradiation and load resistance," *IEEE Transactions on Industrial Informatics*, vol. 11, no. 1, pp. 176–186, 2015.

[24] S. Patel and W. Shireen, "Fast converging digital MPPT control for photovoltaic (PV) applications," in *2011 IEEE power and energy society general meeting*, pp. 1–6, Detroit, MI, USA, July 2011.

[25] M. Sokolov and D. Shmilovitz, "Load line emulation based maximum power point tracking," in *2008 IEEE power electronics specialists conference*, pp. 4098–4101, Rhodes, Greece, June 2008.

[26] T. Sruthy and F. Mohan, "Fast-converging MPPT technique for Photovoltaic system using dsPIC controller," in *2017 11th International Conference on Intelligent Systems and Control (ISCO)*, pp. 140–144, Coimbatore, India, January 2017.

[27] J. Ahmed and Z. Salam, "A modified P&O maximum power point tracking method with reduced steady-state oscillation and improved tracking efficiency," *IEEE Transactions on Sustainable Energy*, vol. 7, no. 4, pp. 1506–1515, 2016.

[28] X. S. Li, H. Q. Wen, L. Jiang, W. Xiao, Y. Du, and C. Zhao, "An improved MPPT method for PV system with fast-converging speed and zero oscillation," *IEEE Transactions on Industry Applications*, vol. 52, no. 6, pp. 5051–5064, 2016.

[29] H. Abouadane, A. Fakkar, Y. Elkouari, and D. J. E. P. Ouoba, "Performance of a new MPPT method for photovoltaic systems under dynamic solar irradiation profiles," *Energy Procedia*, vol. 142, pp. 538–544, 2017.

[30] H. Malek and Y. Q. Chen, "BICO MPPT: a faster maximum power point tracker and its application for photovoltaic panels," *International Journal of Photoenergy*, vol. 2014, Article ID 586503, 9 pages, 2014.

[31] R. X. Fan, J. R. Miao, W. B. Wang, and D. Xie, "Quick MPPT method of centralized PV inverter," *Electric Machines and Control*, vol. 23, no. 7, pp. 113–119, 2019.

[32] J. Ahmed and Z. Salam, "An enhanced adaptive P&O MPPT for fast and efficient tracking under varying environmental conditions," *IEEE Transactions on Sustainable Energy*, vol. 9, no. 3, pp. 1487–1496, 2018.

[33] K. Ishaque, Z. Salam, and H. Taheri, "Simple, fast and accurate two-diode model for photovoltaic modules," *Solar Energy Materials and Solar Cells*, vol. 95, no. 2, pp. 586–594, 2011.

[34] "Solarex MSX60 and MSX-64 photovoltaic modules datasheet," https://www.solarelectricsupply.com/media/custom/upload/Solarex-MSX64.pdf.

[35] T. K. Soon, S. Mekhilef, and A. Safari, "Simple and low cost incremental conductance maximum power point tracking using buck-boost converter," *Journal of Renewable and Sustainable Energy*, vol. 5, no. 2, pp. 1–13, 2013.

[36] R. W. Erickson and D. Maksimovic, *Fundamentals of Power Electronics*, Springer Science & Business Media, 2007.